THE JOURNAL OF BIOLOGICAL CHEMISTRY VOL. 290, NO. 35, pp. 21642–21651, August 28, 2015

Mac-1 Regulates IL-13 Activity in Macrophages by Directly Interacting with IL-13Rα1*

Received for publication, February 16, 2015, and in revised form, June 22, 2015 Published, JBC Papers in Press, July 9, 2015, DOI 10.1074/jbc.M115.645796

Chunzhang Cao[‡], Juanjuan Zhao[‡], Emily K. Doughty[§], Mary Migliorini[¶], Dudley K. Strickland[¶], Maricel G. Kann[§], and Li Zhang[‡1]

From the Departments of [‡]Physiology and [¶]Surgery, Center for Vascular and Inflammatory Diseases, the University of Maryland, School of Medicine, Baltimore, Maryland 21201 and the [§]Department of Biological Sciences, University of Maryland, Baltimore County, Baltimore, Maryland 21250

Background: Mac-1 strongly suppresses IL-13-induced JAK/STAT activation in macrophages, but the mechanism is unknown.
Results: Our data demonstrate that Mac-1 interacts with the IL-13Rα1 subunit of IL-13R and thereby suppresses IL-13 signaling.
Conclusion: Mac-1 regulates macrophage to foam cell transformation by binding to IL-13Rα1.
Significance: This study identifies a novel interaction and provides a potential mechanism by which Mac-1 safeguards macrophages from foam cell differentiation.

Mac-1 exhibits a unique inhibitory activity toward IL-13-induced JAK/STAT activation and thereby regulates macrophage to foam cell transformation. However, the underlying molecular mechanism is unknown. In this study, we report the identification of IL-13Rα1, a component of the IL-13 receptor (IL-13R), as a novel ligand of integrin Mac-1, using a co-evolution-based algorithm. Biochemical analyses demonstrated that recombinant IL-13Rα1 binds Mac-1 in a purified system and supports Mac-1-mediated cell adhesion. Co-immunoprecipitation experiments revealed that endogenous Mac-1 forms a complex with IL-13Rα1 in solution, and confocal fluorescence microscopy demonstrated that these two receptors co-localize with each other on the surface of macrophages. Moreover, we found that genetic inactivation of Mac-1 promotes IL-13-induced JAK/STAT activation in macrophages, resulting in enhanced polarization along the alternative activation pathway. Importantly, we observed that Mac-1$^{-/-}$ macrophages exhibit increased expression of foam cell differentiation markers including 15-lipoxygenase and lectin-type oxidized LDL receptor-1 both *in vitro* and *in vivo*. Indeed, we found that Mac-1$^{-/-}$ LDLR$^{-/-}$ mice develop significantly more foam cells than control LDLR$^{-/-}$ mice, using an *in vivo* model of foam cell formation. Together, our data establish for the first time a molecular mechanism by which Mac-1 regulates the signaling activity of IL-13 in macrophages. This newly identified IL-13Rα1/Mac-1-dependent pathway may offer novel targets for therapeutic intervention in the future.

High levels of LDL and its associated cholesterol in the circulation are well established risk factors for cardiovascular diseases (1–3). LDL accumulates within the subendothelial space in response to inflammation, where it is converted into oxidized LDL (oxLDL)[2] by reactive oxygen species, myeloperoxidase, and lipoxygenase such as 15-lipoxygenase (15-LO), all of which are secreted by macrophages (3). Subsequently, oxLDL is internalized by these macrophages via specific cell surface receptors, including CD36 (4) and lectin-type oxidized LDL receptor-1 (LOX-1) (5), and transforms macrophages into foam cells. Accumulation of fat-laden foam cells in the vessel wall gives rise to the earliest vascular lesions, which gradually progress into fatty streaks, intermediate lesions, and ultimately atherosclerotic plaques (3, 6). The critical role of foam cell formation in the pathogenesis of atherosclerosis is underscored by the observations that genetic inactivation of 15-LO or LOX-1 in mice protects against the development of severe plaques under hyperlipidemia (5, 7).

Macrophages can polarize along two distinct pathways: stimulation with IFN-γ and lipopolysaccharide generates the classically activated macrophages (also known as M1) that exhibit proinflammatory activities, whereas stimulation with IL-4 or IL-13 generates the alternatively activated macrophages (AAMs or M2) that possess anti-inflammatory properties (8–10). Surprisingly, emerging evidence has implicated a pathological role of AAMs in the early stage of atherosclerosis development (9, 11–13). Indeed, AAMs are found to produce high levels of 15-LO and CD36 under the pathological setting of hyperlipidemia (2, 9, 10) and are thus more susceptible to foam cell transformation than classically activated macrophages (11, 12). Recently, Yakubenko *et al.* (9, 14) reported

* This work was supported by National Institute of Health Grants NHLBI HL054710 and NINDS NS082607 (to L. Z.); National Institutes of Health K22CA143148 (to M. G. K.) and American Heart Association Grant 14GRNT20510058 (to L. Z.). The authors declare that they have no conflicts of interest with the contents of this article.

[1] To whom correspondence should be addressed: Dept. of Physiology, Center for Vascular and Inflammatory Diseases, University of Maryland School of Medicine, 800 W. Baltimore St., Baltimore, MD 21201. Tel.: 410-706-8040; Fax: 410-706-8121; Email: lizhang@som.umaryland.edu.

[2] The abbreviations used are: oxLDL, oxidized LDL; 15-LO, arachidonate 15-lipoxygenase; AAM, alternatively activated macrophage; corr. coef., correlation coefficient; IL-13R, IL-13 receptor; IL-13Rα1, IL-13R subunit α1; LDLR, LDL receptor; LOX-1, lectin-like oxidized LDL receptor-1; Mac-1, macrophage antigen 1; qRT-PCR, quantitative real-time RT-PCR; NIF, neutrophil inhibitor factor.

that integrin Mac-1 (CD11b/CD18 or $\alpha_M\beta_2$) functions to suppress IL-13-induced JAK/STAT activation in macrophages and reduces their uptake of oxLDL *in vitro*, suggesting that Mac-1 plays a regulatory role in foam cell development. However, the molecular mechanism by which Mac-1 inhibits IL-13-induced JAK/STAT activation in macrophages is unknown.

In this work, we identified IL-13Rα1, a subunit of the heterodimeric IL-13R, as a novel biological partner of Mac-1, using an unbiased co-evolution-based algorithm. Subsequently, we confirmed direct binding between these two receptors using purified full-length Mac-1 and recombinant IL-13Rα1. We also showed by co-immunoprecipitation that endogenous Mac-1 and IL-13Rα1 form a complex in solution and showed by confocal fluorescence microscopy that they reside in proximity on the cell surface. Biologically, we found that genetic inactivation of Mac-1 enhances IL-13-induced JAK/STAT activation in macrophages and promotes their polarization. Furthermore, we found that the absence of Mac-1 on macrophages increases their expression of foam cell differentiation markers. Using an LDLR$^{-/-}$ mouse model of foam cell formation, our data revealed that Mac-1$^{-/-}$ mice develop significantly more foam cells *in vivo*. Together, our study established for the first time a molecular mechanism by which Mac-1 suppresses IL-13-induced macrophage activation and foam cell transformation. Thus, this newly identified IL-13Rα1/Mac-1 interaction could represent a potential target for therapeutical intervention that will not interfere with IL-13R-medaited immunity or Mac-1-dependent host defense functions.

Experimental Procedures

Mice—WT, Mac-1$^{-/-}$, LDLR$^{-/-}$, and Mac-1$^{-/-}$LDLR$^{-/-}$ mice were all in the C57BL/6J background and used at 8–13 weeks of age (20–22 g). WT and LDLR$^{-/-}$ mice were purchased from The Jackson Laboratory. Mac-1$^{-/-}$ mice were kindly provided by Dr. Christie M. Ballantyne, Baylor College of Medicine (Houston, TX) and have been backcrossed to the C57BL/6J background for more than 10 generations. All mice were housed in a pathogen-free facility, and all procedures were performed in accordance with University of Maryland Institutional Animal Care and Use Committee approval.

Antibodies and Reagents—mAb M1/70 for Mac-1 was from eBioscience (San Diego, CA). Function-blocking mAb 38 for LFA-1 was from Fisher Scientific. Rabbit anti-IL-13R1α and rabbit anti-β-actin were from Sigma. Rabbit anti-15-LO and rabbit anti-STAT6 were from Santa Cruz Biotechnology (Dallas, Texas). Rabbit anti-LOX-1 was from GeneTex (Irvine, CA). Rabbit anti-CD18 cytoplasmic domain ARC22 was prepared as described (15). Rabbit anti-phosphorylated STAT6 (Tyr-641) antibody was from Cell Signaling (Danvers, MA).

Prediction of Protein-Protein Interactions—All protein sequences for the complete genomes of 184 species were downloaded from the National Center for Biotechnology Information (NCBI) Entrez database (16). The set of species contained 130 eukaryotes, 47 prokaryotes, and seven archaea. All sequences for the 184 species were updated on June 2011. Orthologous proteins were identified for each protein in each of the genomes by performing reciprocal BLAST searches (17) against all genomes. For each species, the protein with the smallest average *E*-value (average of the forward and reciprocal *E*-values), with *E*-value $<1 \times 10^{-40}$ and the largest sequence overlap with at least 80% alignment overlap, was selected as the ortholog of protein P for that species.

Calculating Distance Matrices—Multiple sequence alignments for each protein within the pairs of interacting and non-interacting proteins and their corresponding orthologs were obtained using MUSCLE version 3.52 (18). From these multiple sequence alignments, the distance matrices for each protein set were estimated using the ClustalW suite with default parameters (19).

Estimating Correlation Coefficients—For each protein pair from the interacting and non-interacting sets, the correspondence between their evolutionary histories was measured by computing the correlation between the distance matrices of each protein (the Mirrortree approach) (20). For two proteins *A* and *B* with *n* species in common (where $n \geq 9$), let us denote $A_{i,j}$ as the distance between species *i* and *j* for protein *A*; and $B_{i,j}$ for protein *B*. The linear correlation coefficient (corr. coef. or CC_{AB}) between their distance vectors was calculated using the standard Pearson's corr. coef.

$$CC_{AB} = \frac{\sum_{i=1}^{n=1}(A_{i,j} - \bar{A}) \times (B_{i,j} - \bar{B})}{\sqrt{\sum_{i=1}^{n=1}\sum_{j=i+1}^{n}(A_{i,j} - \bar{A})^2} \times \sqrt{\sum_{i=1}^{n=1}\sum_{j=i+1}^{n}(B_{i,j} - \bar{B})^2}} \quad \text{(Eq. 1)}$$

where $\bar{A}$ and $\bar{B}$ are the means of $A_{i,j}$ and $B_{i,j}$ respectively.

Correcting for Speciation—As shown by Pazos *et al.* (21) and Sato *et al.* (22), prediction of protein interactions using co-evolutionary analysis is greatly improved by excluding the background co-evolutionary signal from phylogenetic relationships (signal from speciation). The signal from speciation for species *i* and *j*, represented by matrix $S_{i,j}$, was computed by averaging the evolutionary distance matrices of all proteins in species *i* with their orthologs in species *j*. To estimate the corr. coef. with this correction, the distance matrices $A_{i,j}$ and $B_{i,j}$ in Eq. 1 were replaced by $A'_{i,j}$ and $B'_{i,j}$ where $A'_{i,j} = A_{i,j} - S_{i,j}$ and $B'_{i,j} = B_{i,j} - S_{i,j}$.

Preparation of Peritoneal Macrophages—Mice were injected intraperitoneally with 4% thioglycollate. Four days later, peritoneal macrophages were collected by lavages with PBS. After lysis of red blood cells with ammonium chloride (8.3 g/liter in 10 mM Tris-HCl, pH 7.4), peritoneal cells were plated on 10-cm tissue culture Petri dishes in 10% FBS in DMEM and incubated in a humidified incubator with 5% CO_2 at 37 °C for 2–4 h. Adherent macrophages were collected, and their purity was verified by flow cytometry based on positive staining for F4/80 and M1/70 and by morphological examination of Hema 3 (Fisher Scientific)-stained smears prepared with a Cytospin (Shandon).

Alternative Activation of Macrophages and qRT-PCR—Peritoneal macrophages were treated with or without 4 nM IL-13 for various times, ranging from 5 min to 3 days. STAT6 activation was assessed by Western blot using phospho-STAT6-specific antibody. Total STAT6 protein and β-actin were used as loading controls. Macrophage polarization along the alternative

TABLE 1
Primers used for qRT-PCR

β-Actin	NM_007393	Forward (5′ to 3′)	AGTGTGACGTTGACATCCGT
		Reverse (5′ to 3′)	TGCTAGGAGCCAGAGCAGTA
YM-1	NM_009892	Forward (5′ to 3′)	TCTATGCCTTTGCTGGAATG
		Reverse (5′ to 3′)	CAGGTCCAAACTTCCATCCT
YM-2	NM_145126	Forward (5′ to 3′)	CCTTTGCTGGGATGAAGAAT
		Reverse (5′ to 3′)	CCAAACTTCCATCCTCCAAT
FIZZ1	NM_020509	Forward (5′ to 3′)	AGGAACTTCTTGCCAATCCA
		Reverse (5′ to 3′)	ACAAGCACACCCAGTAGCAG
Arginase-1	NM_007482	Forward (5′ to 3′)	ACAACCAGCTCTGGGAATCT
		Reverse (5′ to 3′)	TGTACACGATGTCTTTGGCA
Lox-1	NM_138648	Forward (5′ to 3′)	TGACTCTGGTCATCCTCTGC
		Reverse (5′ to 3′)	TGCTGAGTAAGGTTCGCTTG
15-LO	NM_009660	Forward (5′ to 3′)	TGGTTCTGCAACTGGATTTC
		Reverse (5′ to 3′)	GGCCTTGAGAGTCTTCAACC
IL-6	NM_031168	Forward (5′ to 3′)	CTCTGGGAAATCGTGGAAAT
		Reverse (5′ to 3′)	CCAGTTTGGTAGCATCCATC

activation pathway was assessed by quantitative real-time RT-PCR (qRT-PCR) based on expression of specific markers, including Arginase-1, FIZZ1, YM1, and YM2. Briefly, total RNA was extracted from peritoneal macrophages using the Absolutely RNA miniprep kit (Stratagene) according to the manufacturer's instructions. One microgram of total RNA was used for cDNA synthesis using SuperScript II and random hexamers (Invitrogen). qRT-PCR was performed on an ABI Prism 7500 HT sequence detection system (Applied Biosystems), using specific primer pairs (Table 1). The PCR reaction was done in a 25-μl solution containing 12.5 μl of SYBR® Green PCR master mix, 10 ng of cDNA, and 400 nM of each primer, with the following settings: activation of the AmpliTaq Gold® polymerase at 95 °C for 10 min and 40 cycles of 95 °C for 15 s and 60 °C for 1 min. The melting curve was analyzed using the ABI software, and quantification of gene expression was done based on the $2^{-\Delta\Delta Ct}$ method (RQ Manager 1.4). Each experiment was run in duplicates. All data were normalized to β-actin expression in the same cDNA set.

Ligand Binding—Binding of recombinant IL-13Rα1 to purified full-length Mac-1 was carried out in 96-well microtiter plates. Detergent-solubilized Mac-1 was purified from Mac-1-expressing HEK293 cells (23) by affinity chromatography using mAb LM2/1-coupled agarose. The purity of Mac-1 was verified by SDS-PAGE and by its ability to bind conformation-dependent mAbs (data not shown). Fifty microliters of 10 μg/ml purified Mac-1 in 100 mM KCl, 3 mM $MgCl_2$, 10 mM PIPES, pH 7.0, were used to coat the wells of 96-well microplates at 4 °C overnight. The plate was washed and blocked with 1% BSA. Recombinant mouse IL-13Rα1, which contains a histidine tag at its C terminus (Leinco Technologies Inc.), was added at different concentrations (0–2 μM) in the above buffer plus 0.1% BSA. After incubation at 37 °C for 2 h, the plate was washed, and bound IL-13Rα1 was detected using HisProbe-HRP (Thermo Scientific) with its substrate 3,3′,5,5′-tetramethylbenzidine, measuring absorbance at 450 nm. The binding curve was fitted to the Michaelis-Menten equation based on a single binding site model using SigmaPlot (Systat Software, Inc., San Jose, CA).

Cell Adhesion Assays—Cell adhesion was conducted based on our published methods (23). Briefly, 24-well polystyrene microtiter plates were coated with increasing concentrations of recombinant mouse IL-13Rα1, BSA, or 10 μg/ml ICAM-1-Fc (24). The plates were blocked with 400 μl of 0.05% polyvinylpyrrolidone in Dulbecco's PBS. A total of 2×10^6 Mac-1-expressing HEK293 cells in Hanks' balanced salt solution containing 1 mM Ca^{2+} and 1 mM Mg^{2+} in the presence or absence of 50 nM neutrophil inhibitor factor (NIF; a Mac-1-specific antagonist (25)) or LFA-1-expressing HEK293 cells in Hanks' balanced salt solution containing 2 mM EGTA and 2 mM Mg^{2+} with or without 10 μg/ml mAb 38 (a LFA-1 function-blocking mAb) were added to each well. After incubation at 37 °C for 30 min, non-adherent cells were removed by three washes with Dulbecco's PBS and adherent cells were stained with Crystal Violet. Cell adhesion was quantified based on absorption at 595 nm.

Co-immunoprecipitation—Co-immunoprecipitation experiments were conducted based on our published methods (26). WT peritoneal macrophages were stimulated with IL-13, washed, and then lysed. The cell lysates were immunoprecipitated using a rabbit anti-IL-13Rα1 antibody, and the immunoprecipitates were separated on 10% SDS-PAGE, transferred to PVDF membrane, and probed with anti-CD18 antibody ARC22 (15). Equal loading was verified by the presence of equal amounts of CD18 and β-actin in the cell lysates.

Confocal Laser Scanning Fluorescence Microscopy—Co-localization between IL-13Rα1 and Mac-1 was determined by confocal fluorescence microscopy based on our published method (26). Peritoneal macrophages were seeded on multi-coverslips overnight. The cells were washed with PBS and fixed with 4% paraformaldehyde in PBS for 30 min at room temperature. After blocking with 5% bovine serum albumin in PBS at room temperature for 30 min, these cells were incubated with 20 μg/ml rabbit anti-IL-13Rα1 antibody and 20 μg/ml rat anti-Mac-1 mAb (M1/70) in 1% bovine serum albumin in PBS at room temperature for 60 min. After washing, these different coverslips were incubated with Alexa Fluor 488-conjugated goat anti-rabbit IgG and Alexa Fluor 568-conjugated goat anti-rat IgG (Molecular Probes). Non-immune rabbit and rat IgGs were used as specificity controls. The stained macrophages were analyzed using a Bio-Rad Radiance 2000 confocal laser scanning fluorescence microscope system equipped with a Nikon Eclipse E800 upright light microscope. The images

were collected using 100× oil objectives with a slice thickness of 2.6 μm.

Foam Cell Formation in Vivo—The formation of foam cells *in vivo* was investigated based on published methods (27) with minor modifications. Briefly, Mac-1$^{-/-}$LDLR$^{-/-}$ mice and their LDLR$^{-/-}$ littermates were fed a high fat "Western" diet (21% fat and 0.2% cholesterol) for 5 weeks. Peritoneal macrophages were prepared from these mice by intraperitoneal injection of 4% thioglycollate, followed by peritoneal lavage 4 days later. Foam cells within the collected peritoneal cells were identified by staining the fat droplets within the cytosol with Oil Red O following centrifuging in the Cytospin. To quantify the amount of cholesterol accumulated within these foam cells, peritoneal cells were pelleted at 1000 rpm for 7 min, extracted in 500 μl of isopropanol by sonication (2 × 10 s), and then centrifuged at 14,000 rpm for 10 min. The pellet was used to determine the amount of total protein by Bio-Rad protein assay. The supernatant was assayed for cholesterol using Amplex Red kit (Invitrogen) according to the manufacturer's protocol. Free cholesterol was determined by omitting the cholesterol esterase. Total cholesterol was determined in the presence of the cholesterol esterase. Cholesterol esters were calculated from the difference in total and free cholesterol. Data are plotted as mg of cholesterol per mg of protein.

Statistical Analysis—Statistical analyses were performed using two-tailed Student's *t* test. *p* values less than 0.05 were considered significant.

Results

Co-evolution between Mac-1 and IL-13Rα1—Recently, Yakubenko *et al.* (9, 14) reported that Mac-1 suppresses IL-13-induced JAK/STAT activation in macrophages and reduces their uptake of oxLDL *in vitro*; however, the molecular mechanism underlying this unique regulatory function of Mac-1 is not yet established. To identify potential biological partners that confer the inhibitory activity of Mac-1 toward IL-13-induced macrophage activation, we used an unbiased informatics-based method, termed Mirrortree (28–30), to predict protein-protein interactions. The premise of Mirrortree is that biological partners, such as parasite/host, must change in sync during evolution to maintain their interdependence (28). Accordingly, we downloaded the entire protein sequences encoded in 184 different species from the NCBI Entrez database (16) and identified the orthologous protein representatives for each species. Multiple sequence alignments for each protein within the pairs of interacting and non-interacting proteins and their corresponding orthologs were then calculated using MUSCLE version 3.52 (18). From these multiple sequence alignments, the distance matrices for each protein set were estimated using the ClustalW suite with default parameters (19). Linear correlation coefficients for each protein pair from the interacting and non-interacting sets was calculated using the standard Pearson's correlation coefficient. Finally, background co-evolutionary signals, *e.g.* due to speciation, were excluded from phylogenetic relationships, based on published methods (21, 22).

One of the proteins that co-evolve with Mac-1 is IL-13Rα1 (corr. coef. = 0.76×10^{-40}). Fig. 1 shows the concerted changes in protein sequence of Mac-1 and IL-13Rα1 during a million years of evolution, suggesting that these two proteins may interact with each other to maintain important biological functions. IL-13Rα1 associates with IL-4Rα and forms the heterodimeric receptor IL-13Rα1/IL-4Rα (IL-13R) that is responsible for IL-13-induced intracellular signaling. Accordingly, we hypothesized that Mac-1 suppresses IL-13-induced macrophage activation and its subsequent polarization by binding to IL-13Rα1 on the macrophage surface.

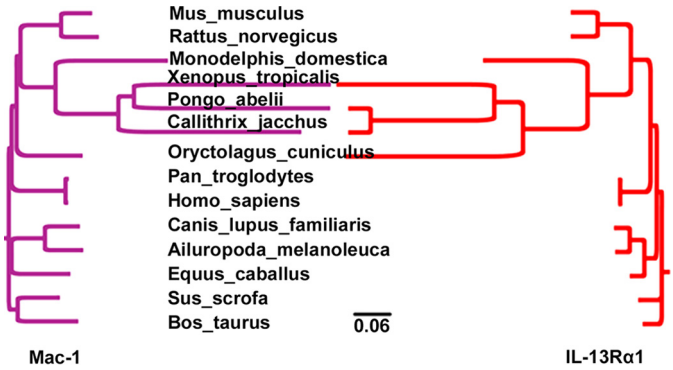

FIGURE 1. **Co-evolution between Mac-1 and IL-13Rα1.** A Mirrortree-based algorithm was used to calculate changes in the protein sequences of Mac-1 and IL-13Rα1 during evolution. The database contains the complete genome data of 184 species, including 130 eukaryotes, 47 prokaryotes, and seven archaea. The calculated correlation coefficient between Mac-1 and IL-13Rα1 is 0.76×10^{-40}. The major changes of Mac-1 and IL-13Rα1 during evolution are shown. *Scale bar:* 0.06 million years.

Direct Interaction between purified Mac-1 and Recombinant IL-13Rα1—To test our hypothesis, we first examined whether Mac-1 interacts directly with IL-13Rα1 in a purified system. We isolated full-length Mac-1 from Mac-1-expressing HEK293 cells by affinity chromatography. Purified Mac-1 was then incubated with recombinant soluble IL-13Rα1 in a 96-well microtiter plate, with or without the addition of a neutralizing anti-IL-13Rα1 antibody. We found that IL-13Rα1 bound immobilized Mac-1 in a dose-dependent manner with a K_d of ~5 μM (Fig. 2*A*), which could be inhibited by an anti-IL-13Rα1 antibody, thus verifying the specificity of the binding assay. Next, we evaluated whether IL-13Rα1 can support Mac-1-mediated cell adhesion. We coated 24-well microtiter plates with increasing concentrations of IL-13Rα1 or a control protein BSA. After blocking the plates, Mac-1- or LFA-1-expressing HEK293 cells were added in the presence or absence of a Mac-1-specific antagonist NIF (25) or LFA-1-blocking mAb 38 and incubated at 37 °C for 30 min. The plates were washed to remove non-adherent cells and the adherent cells were quantified. Fig. 2*B* shows that IL-13Rα1 supported adhesion of Mac-1-expressing HEK293 cells in a dose-dependent manner with an EC_{50} of ~0.5 μM. In comparison, little adhesion of Mac-1/HEK293 cells was observed to BSA-coated wells. Moreover, the addition of a Mac-1-specific antagonist NIF blocked more than 65% Mac-1/HEK293 cell adhesion to IL-13Rα1, thus verifying specificity. Furthermore, we found that LFA-1/HEK293 cells adhered strongly to ICAM-1, which could be inhibited by mAb 38; however, they failed to adhere to IL-13Rα1 (Fig. 2*C*). As expected, Mac-1/HEK293 cells adhered to both ICAM-1 and IL-13Rα1, both of which could be blocked by NIF. These results demonstrate that Mac-1 interacts specifically with IL-13Rα1, thus

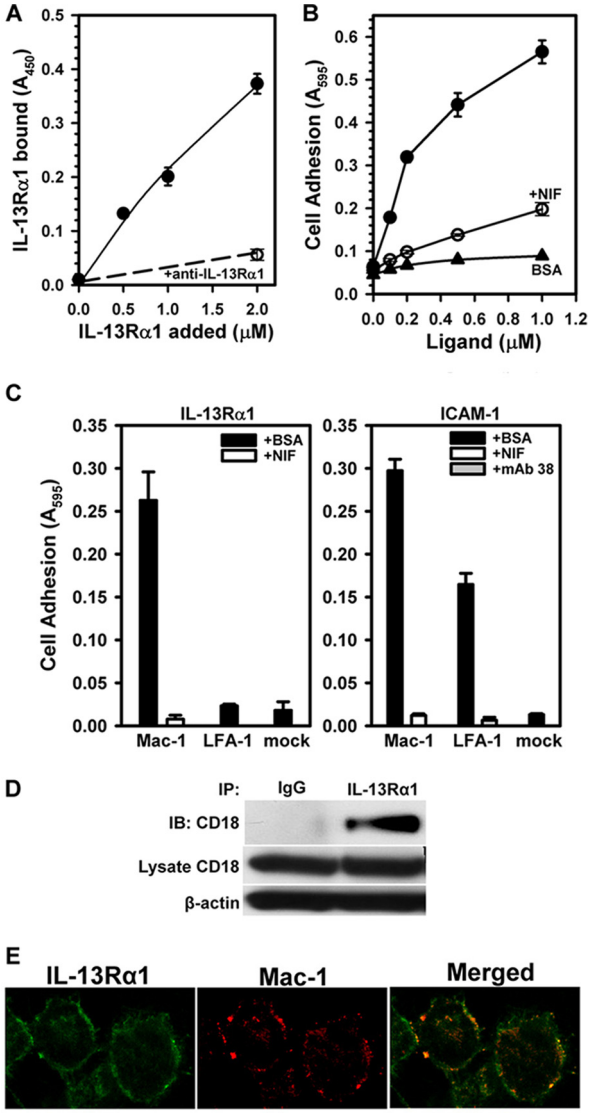

FIGURE 2. **Mac-1 interacts with IL-13Rα1 on the surface of macrophages.** *A*, ligand binding. Increasing concentrations of recombinant soluble IL-13Rα1 (contains a C-terminal His tag) were added in 96-well microtiter plates, which were precoated with purified Mac-1, in the absence (●) or presence (○) of an IL-13Rα1-neutralizing antibody. Bound IL-13Rα1 was detected using a His-Probe-HRP conjugate and its substrate 3,3′,5,5′-tetramethylbenzidine, measuring absorbance at 450 nm. Data shown are means ± S.D. of duplicate experiments. *B*, cell adhesion. Mac-1-expressing HEK293 cells were added to 24-well microtiter plates, which were precoated with increasing concentrations of IL-13Rα1 (●) or BSA (▲), in the absence or presence of a Mac-1-specific antagonist NIF (○). After incubation at 37 °C for 30 min, non-adherent cells were removed and adherent cells were stained with Crystal violet. Cell adhesion was quantified based on absorption at 595 nm. Data shown are means ± S.D. of duplicate experiments. *C*, Mac-1- or LFA-1-expressing HEK293 cells were added to 24-well microtiter plates, which were precoated with IL-13Rα1, ICAM-1, or BSA, in the absence or presence of NIF or mAb 38. Cell adhesion was carried out as above. Mock-transfected HEK293 cells were used as a control. Data shown are means ± S.D. of duplicate experiments. *D*, co-immunoprecipitation. Total lysates of peritoneal macrophages were incubated with an anti-IL-13Rα1 antibody or a control IgG and then immunoprecipitated (*IP*) with protein A-agarose. Immunoprecipitates were separated on 10% SDS-PAGE and subjected to immunoblot (*IB*) with an anti-CD18 antibody ARC22. Total cell lysates were probed for CD18 and β-actin to verify equal protein loading. *E*, co-localization. Peritoneal macrophages were stained with a rabbit anti-IL-13Rα1 antibody and a rat anti-Mac-1 mAb (M1/70), followed by Alexa Fluor 488-anti-rabbit IgG and Alexa Fluor 568-anti-rat IgG. Specificity was verified using non-immune rabbit and rat IgGs (data not shown). Representative images shown were taken with 100× objective oil lens with a slice thickness of 2.6 μm. Co-localization between IL-13Rα1 (in *green*) and Mac-1 (in *red*) was shown in *yellow color* in the merged image.

supporting our hypothesis that Mac-1 modulates the function of IL-13 by interacting with its receptor IL-13R.

Endogenous Mac-1 and IL-13Rα1 Form a Complex in Solution—To test whether Mac-1 and IL-13Rα1 interact with each other when expressed on macrophages, we conducted co-immunoprecipitation experiments using primary macrophages harvested from thioglycollate-treated mice. We collected peritoneal macrophages and prepared cell lysates. IL-13Rα1 was then immunoprecipitated with its specific antibody. After separation of the immunoprecipitates on SDS-PAGE, the presence of Mac-1 in the immunoprecipitates was determined by Western blot using an anti-CD18 antibody ARC22 (15). We found that Mac-1 was pulled down by an anti-IL-13Rα1 antibody but not by a control IgG (Fig. 2*D*), demonstrating that Mac-1 and IL-13Rα1 formed a complex in solution.

Mac-1 Is Associated with IL-13Rα1 on the Surface of Macrophages—To determine whether Mac-1 and IL-13Rα1 associate with one another on the cell surface, peritoneal macrophages were stained with a rabbit anti-IL-13Rα1 antibody and a rat anti-Mac-1 antibody and then incubated with their corresponding secondary antibody conjugated with Alexa Fluor 488 or Alexa Fluor 568, respectively. The stained macrophages were analyzed by confocal fluorescence microscopy. We found that IL-13Rα1 co-localized with Mac-1 (Fig. 2*E*, *yellow color* in the merged image), suggesting that these two receptors reside proximally on the cell surface.

Genetic Inactivation of Mac-1 Enhances IL-13-induced JAK/STAT Activation—IL-13Rα1 is a subunit of IL-13R. Stimulation of this heterodimeric IL-13R receptor by IL-13 leads to activation of the JAK/STAT pathway (8, 31). To investigate whether Mac-1 association with IL-13Rα1 plays a functional role in IL-13R signaling, we stimulated WT and Mac-$1^{-/-}$ macrophages with IL-13. Activation of the IL-13R signaling pathway was measured by Western blot using an antibody that specifically recognizes the phosphorylated form of STAT6 (at Tyr-641). The results showed that treatment of macrophages with IL-13 resulted in a time-dependent increase in phosphorylated STAT6, plateauing at 30 min (Fig. 3*A*). Genetic inactivation of Mac-1 significantly enhanced STAT6 phosphorylation as compared with their WT counterparts (Fig. 3*A*). These data demonstrated that Mac-1 functions to suppress IL-13R signaling in IL-13-stimulated macrophages.

Deficiency of Mac-1 Promotes Macrophage Polarization along the Alternative Activation Pathway—IL-13 signaling promotes macrophage polarization along the alternative pathway, generating AAMs (8). To determine whether the increased JAK/STAT activation in Mac-$1^{-/-}$ macrophages leads to enhanced alternative activation, we quantified the levels of several AAM markers, including Arginase-1, FIZZ1, YM-1, and YM2 (8), by qRT-PCR. The results showed that Mac-$1^{-/-}$ macrophages had higher transcription levels of these four AAM markers, both in the absence and in the presence of IL-13 stimulation, as compared with WT cells (Fig. 3*B*). We also observed that Mac-$1^{-/-}$ macrophages expressed significantly higher levels of IL-6, a proinflammatory cytokine (Fig. 3*B*).

Mac-1 Suppresses Macrophage Expression of Foam Cell Differentiation Markers in Vitro and in Vivo—To investigate whether Mac-1 deficiency predisposes macrophages to foam

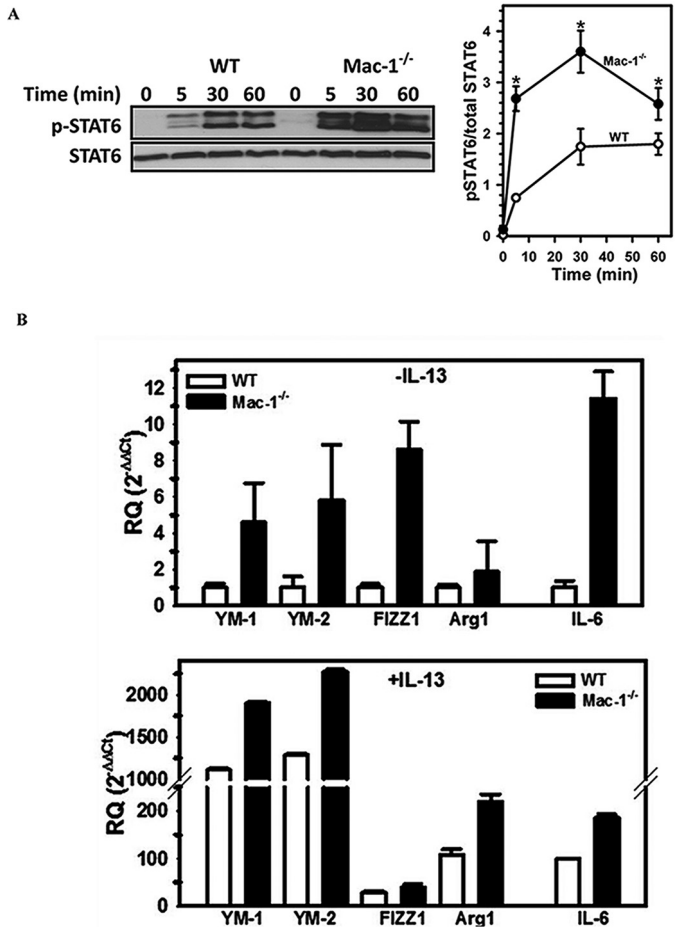

FIGURE 3. **Genetic inactivation of Mac-1 enhances IL-13 signaling activity and promotes macrophage polarization.** *A*, WT or Mac-1$^{-/-}$ peritoneal macrophages were treated with 4 nM IL-13 for the indicated time at 37 °C. Tyrosine phosphorylation of STAT6 (*p-STAT6*) was determined by Western blot using an anti-phospho-STAT6 antibody. Equal sample loading was verified using an anti-total STAT6 antibody. Quantification of STAT6 phosphorylation was done using ImageJ (National Institutes of Health). Data shown are means ± S.D. of triplicate experiments. *, $p < 0.05$, WT *versus* Mac-1$^{-/-}$. *B*, WT (*open bars*) or Mac-1$^{-/-}$ (*filled bars*) peritoneal macrophages were stimulated without (*upper panel*) or with (*lower panel*) 4 nM IL-13 for 24 h. Gene transcription was quantified by qRT-PCR using PCR primers specific for YM-1, YM-2, FIZZ1, Arginase-1 (Arg1), and IL-6 (Table 1). Data shown are means ± S.D. of duplicate experiments. *RQ*, relative quantitation.

cell differentiation, we evaluated the expression of several differentiation markers for foam cells. The results showed that Mac-1$^{-/-}$ macrophages exhibited increased gene transcription of 15-LO and LOX-1, both of which are critical to foam cell formation, with or without IL-13 stimulation (Fig. 4*A*). Western blot analysis showed that the protein levels of 15-LO and LOX-1 in macrophages increased as well upon IL-13 stimulation, but they exhibited distinct patterns: the level of 15-LO was up-regulated early but peaked on Day 1, whereas the LOX-1 level continued to rise on Day 3 (Fig. 4*B*). Importantly, we found that Mac-1$^{-/-}$ macrophages exhibited higher protein levels for both 15-LO and LOX-1 antigen on Day 1 and Day 3 (Fig. 4*B*), which agreed well with their increased gene transcription. No significant effect of Mac-1 deficiency was observed on the expression of CD36, SR-A1, or SR-BI (data not shown).

To test whether Mac-1 deficiency results in an enhanced foam cell development *in vivo*, we employed an LDLR$^{-/-}$ mouse model of foam cell formation (27). We crossed Mac-1$^{-/-}$ mice with LDLR$^{-/-}$ mice and then fed Mac-1$^{-/-}$ LDLR$^{-/-}$ mice and their littermate LDLR$^{-/-}$ controls a high fat diet for 5 weeks. After intraperitoneal injection of thioglycollate, peritoneal macrophages were harvested on Day 4 by lavage. Expression of 15-LO and LOX-1 in the peritoneal macrophages was determined by qRT-PCR. We found that macrophages derived from Mac-1$^{-/-}$LDLR$^{-/-}$ mice exhibited significantly higher transcription levels of 15-LO, LOX-1, and IL-6 than those of their WT counterparts (Fig. 4*C*).

Mac-1-deficient Mice Exhibit Increased Foam Cell Formation in Vivo—To directly investigate whether Mac-1-deficient mice develop more foam cells *in vivo*, we subjected the peritoneal cells obtained from the above high fat diet-fed LDLR$^{-/-}$ and Mac-1$^{-/-}$LDLR$^{-/-}$ mice to Oil Red O staining. The results showed that peritoneal macrophages from Mac-1$^{-/-}$LDLR$^{-/-}$ mice contained more fat droplets than those from LDLR$^{-/-}$ littermates (Fig. 5*A*; red color), indicating that Mac-1 deficiency enhanced foam cell transformation. To quantify the amount of foam cells generated *in vivo*, we determined the total cholesterol content of the peritoneal macrophages harvested from the above mice. The results showed that the cells from Mac-1$^{-/-}$ LDLR$^{-/-}$ mice contained significantly higher levels of total cholesterol and cholesterol ester than those from LDLR$^{-/-}$ littermates (Fig. 5*B*). No difference in free cholesterol contents was observed between the macrophages from Mac-1$^{-/-}$ LDLR$^{-/-}$ mice and their littermate controls (Fig. 5*B*).

Discussion

A major step in the development of vascular diseases, such as atherosclerosis, is the generation of foam cells within the subendothelial space, which marks the formation of the earliest vascular lesions (1, 6). Recent studies demonstrated that Mac-1, a major leukocyte integrin expressed on macrophages and macrophage-derived foam cells, exhibits potent inhibitory activities toward JAK/STAT activation in IL-13-stimulated macrophages, which reduces their ability to uptake oxLDL *in vitro* (9, 14). However, the molecular mechanism by which Mac-1 inhibits IL-13 signaling in macrophages is still unknown. Here, we report for the first time the identification of IL-13Rα1 as a biological partner based on a combination of bioinformatics and biochemical approaches. Our results demonstrate that Mac-1 directly interacts with IL-13Rα1 and thereby suppresses IL-13-induced JAK/STAT activation. Hence, this study establishes a novel mechanism by which Mac-1 regulates IL-13 signaling in macrophages, thus suppressing their transformation into foam cells.

Using a Mirrortree-based algorithm, we first observed that Mac-1 co-evolves with IL-13Rα1 during evolution (Fig. 1), suggesting that these two receptors may dependent on each other to function. Next, we confirmed that Mac-1 binds directly to IL-13Rα1 in a purified system using recombinant proteins (Fig. 2*A*). The ability of endogenous Mac-1 and IL-13Rα1 expressed on primary macrophages to interact with each other in solution was verified by co-immunoprecipitation experiments (Fig. 2*D*), and their association on the cell surface was confirmed by confocal fluorescence microscopy (Fig. 2*E*). Biochemical assays demonstrated that the formation of the Mac-1/IL-13R complex

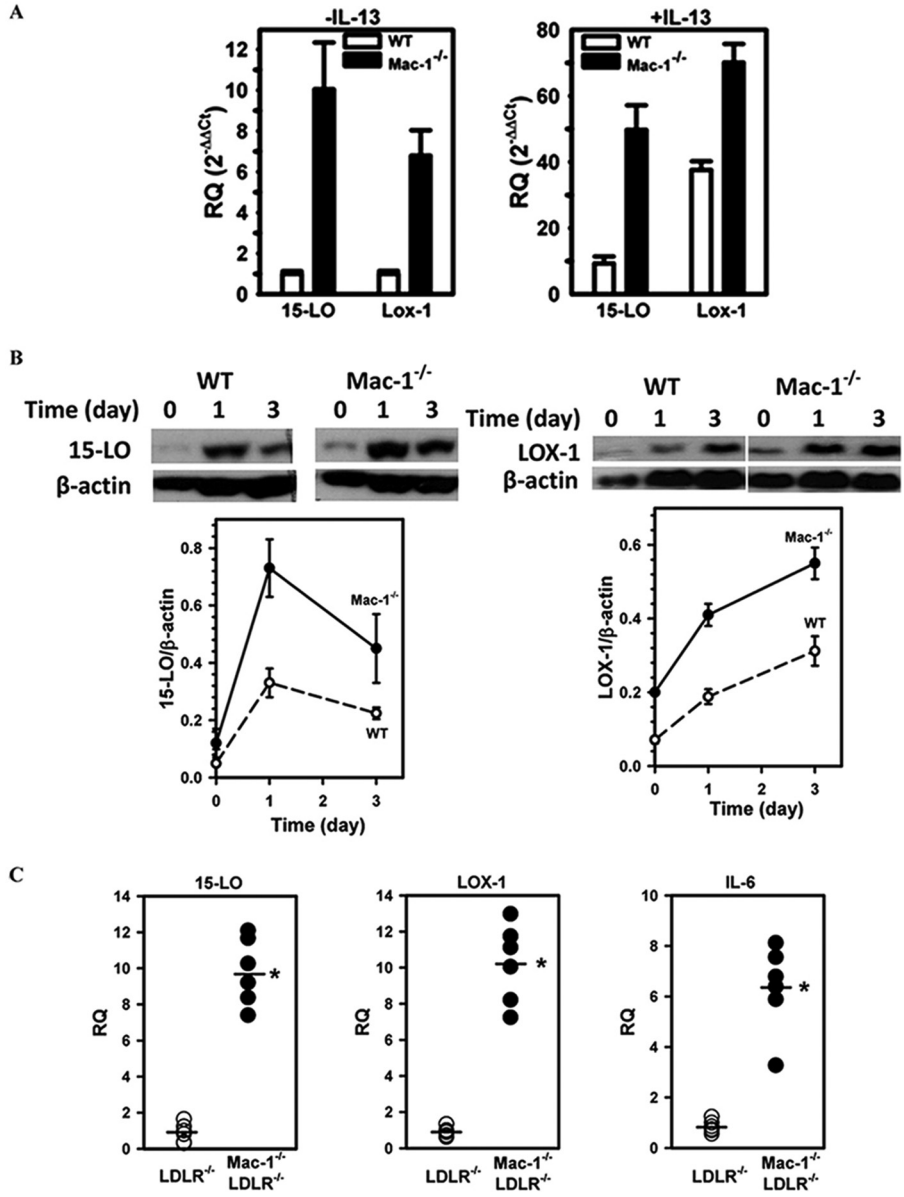

FIGURE 4. **Mac-1 suppresses foam cell differentiation *in vitro* and *in vivo*.** *A*, WT or Mac-1$^{-/-}$ peritoneal macrophages were stimulated *in vitro* without or with 4 nM IL-13 for 24 h. Gene transcription of foam cell differentiation markers LOX-1 and 15-LO was quantified by qRT-PCR. Data shown are means ± S.D. of duplicate experiments. *RQ*, relative quantitation. *B*, WT or Mac-1$^{-/-}$ peritoneal macrophages were treated *in vitro* with 4 nM IL-13 for 0, 1, and 3 days. Production of 15-LO and LOX-1 was determined by Western blot, using their corresponding antibodies. The amount of 15-LO and LOX-1 was quantified by ImageJ (National Institutes of Health) and normalized to the amount of β-actin. Data shown represent means ± S.D. of duplicate experiments. *C*, LDLR$^{-/-}$ and Mac-1$^{-/-}$LDLR$^{-/-}$ littermates were fed a high fat diet for 5 weeks. Peritoneal macrophages were harvested following thioglycollate injection, and gene transcription was analyzed by qRT-PCR. *Open circles*, LDLR$^{-/-}$; *filled circles*, Mac-1$^{-/-}$LDLR$^{-/-}$. All data were normalized to β-actin expression in the same cDNA set. The mean value within each group is shown with a *horizontal bar*. *, $p < 0.05$, LDLR$^{-/-}$ *versus* Mac-1$^{-/-}$LDLR$^{-/-}$, $n = 6$.

on macrophages dampens IL-13-induced JAK/STAT activation (Fig. 3*A*) and thus suppresses macrophage polarization along the alternative activation pathway (Fig. 3*B*). Consequently, our data showed that Mac-1 deficiency predisposes macrophages to foam cell differentiation both *in vitro* and *in vivo* (Fig. 4). Most importantly, we demonstrated that genetic inactivation of Mac-1 promotes the generation of foam cells *in vivo* using an LDLR$^{-/-}$ mouse model of foam cell development (Fig. 5). Together, this study establishes a major role of the Mac-1/IL-13Rα1 interaction in safeguarding macrophages from aberrant foam cell development.

Mac-1 is a leukocyte integrin of the CD18 subfamily and expressed abundantly on macrophages and macrophage-derived foam cells. A unique feature of Mac-1 is its ability to recognize a wide range of diverse protein and non-protein ligands. These unique interactions may underlie the ability of Mac-1 to facilitate both pro-inflammatory and anti-inflammatory responses in a context-dependent manner (32–40). For example, Mac-1 binding of C3bi has been shown to suppress inflammation and induce immune tolerance (41, 42); on the other hand, Mac-1-mediated adhesion to fibrin exacerbates inflammatory diseases (36, 39). Given the suppressive activity of Mac-1 toward IL-13 signaling in macrophages (9, 14), we sought in this work to identify candidate partners of Mac-1 that mediate this unique regulatory activities. To achieve our objective, we developed a computational method to predict protein-

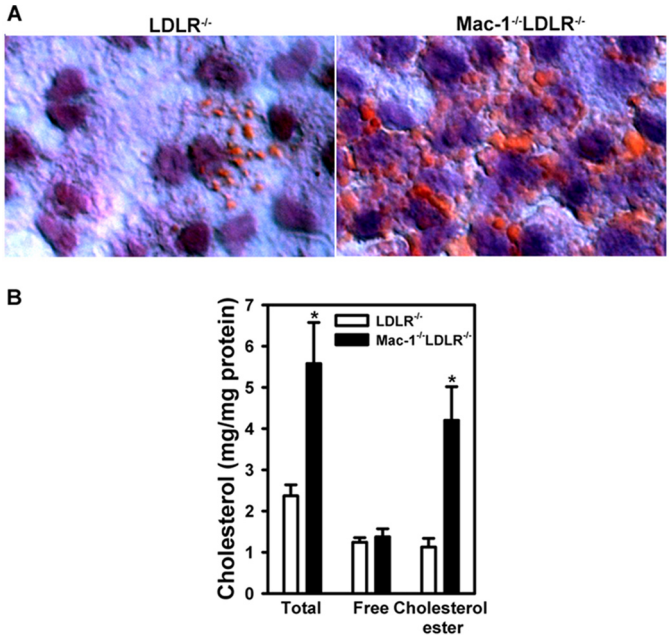

FIGURE 5. **Mac-1 suppresses foam cell development *in vivo*.** LDLR$^{-/-}$ and Mac-1$^{-/-}$LDLR$^{-/-}$ littermates were fed a high fat diet for 5 weeks as above. *A*, peritoneal macrophages were harvested by lavage and stained by Oil Red O to visualize intracellular fat droplets (in *red*). Nucleus was stained with hematoxylin and is shown in *dark blue*. *B*, cholesterol contents of the peritoneal macrophages were quantified by ELISA and normalized to the amount of total protein. Data shown are means ± S.E. *, $p < 0.05$, LDLR$^{-/-}$ *versus* Mac-1$^{-/-}$LDLR$^{-/-}$, $n = 4–5$.

protein interactions, based in part on Mirrortree, using the entire genetic and protein sequence database. This method relies on the conservation of gene order (43, 44), domain/gene fusion (45), and co-evolution (46–48). The assumption behind co-evolution-based Mirrortree methods is that for a given interacting protein pair, sequence changes in one protein are mirrored in the other protein to maintain their interaction and thus biological function. Using this unbiased method, we found that IL-13Rα1, but not IL-4Rα, co-evolves with Mac-1, suggesting that Mac-1 may regulate IL-13 signaling activity in macrophages by interacting with the IL-13Rα1 subunit of the IL-13R. In support of this prediction, we showed that Mac-1 binds IL-13Rα1 directly with a relative low affinity (K_d of ~5 μM; Fig. 2*A*), which could be further enhanced by multivalent receptor-receptor interactions on the cell surface. Indeed, we found that immobilized IL-13Rα1 supported Mac-1-mediated cell adhesion with a relatively higher affinity (EC_{50} of 0.5 μM; Fig. 2*B*). Together, this study identifies IL-13Rα1 as a new ligand of Mac-1 that contributes to its ability to suppress foam cell development, especially in the setting of hyperlipidemia. Finally, as genetic ablation of the Mac-1/IL-13Rα1 interaction leads to enhanced IL-13 signaling (Fig. 3), our data support a working model that Mac-1 association with IL-13Rα1 interferes with the function of the IL-4Rα/IL-13Rα1 heterodimer by sterically hindering IL-13 binding. Experiments to test this hypothesis are currently underway.

Mac-1 and IL-13Rα1 are both composed of multiple independent domains (49, 50). In particular, the α_M subunit of Mac-1 contains an I-domain, a β-propeller, a Thigh domain, two Calf domains, a transmembrane domain, and a cytoplasmic tail (49). Major ligand binding activities have been localized to the I-domain, although other domains may also contribute to the binding of specific ligands. The IL-13Rα1 subunit contains three domains: an N-terminal Ig-like domain (D1) and two Fibronectin-III homologous domains (D2 and D3). All three domains participate directly in IL-13 binding (50). To determine putative domains of Mac-1 and IL-13Rα1 that may interact with each other, we conducted bioinformatics analysis on individual domain pairs that co-evolve. We delineated individual domains within Mac-1 and IL-13Rα1 by introducing "breaks" at the domain boundary during multiple sequence alignments and then performed Mirrortree analysis as discussed above. Several domain pairs were found to co-evolve significantly. A major candidate interacting pair involves the fifth blade of the α_M β-propeller (residues 453–511) with one or more domains of IL-13Rα1, including the D3 domain (resides 233–346; corr. coef. = 0.79×10^{-40}), the D2 domain (residues 129–219; corr. coef. = 0.78×10^{-40}), and/or the D1 domain (residues 27–117; corr. coef. = 0.75×10^{-40}). Other potential interactions include the α_M I-domain (residues 149–324) with the IL-13Rα1 D2 domain (corr. coef. = 0.67×10^{-40}) and the α_M leg region (residues 615–1033) with the IL-13Rα1 D3 domain (corr. coef. = 0.55×10^{-40}). The validity of these predicted interactions needs to be assessed experimentally in the future.

In summary, we have identified IL-13Rα1 as a novel Mac-1 partner based on an unbiased co-evolution-based informatics approach, which was subsequently confirmed by biochemical assays. We demonstrated that Mac-1 interacts with IL-13Rα1 and associates with IL-13R on the surface of macrophages. Genetic inactivation of Mac-1 increases IL-13-induced JAK/STAT activation and predisposes macrophages to foam cell differentiation. Altogether, our study identified a unique mechanism by which Mac-1 protects macrophages against foam cell transformation in disease settings such as hyperlipidemia. This newly identified IL-13Rα1/Mac-1-dependent pathway may offer novel targets for therapeutic intervention in the future.

Author Contributions—C. C. designed, performed, and analyzed the experiments. J. Z. performed animal studies. E. K. D. and M. G. K. conducted bioinformatics analysis. M. M. and D. K. S. measured cholesterol contents of peritoneal macrophages. L. Z. conceived and coordinated the study and wrote the paper. All authors reviewed the results and approved the final version of the manuscript.

References

1. Libby, P., Ridker, P. M., and Hansson, G. K. (2011) Progress and challenges in translating the biology of atherosclerosis. *Nature* **473,** 317–325
2. Ley, K., Miller, Y. I., and Hedrick, C. C. (2011) Monocyte and macrophage dynamics during atherogenesis. *Arterioscler. Thromb. Vasc. Biol.* **31,** 1506–1516
3. Moore, K. J., and Tabas, I. (2011) Macrophages in the pathogenesis of atherosclerosis. *Cell* **145,** 341–355
4. Febbraio, M., Podrez, E. A., Smith, J. D., Hajjar, D. P., Hazen, S. L., Hoff, H. F., Sharma, K., and Silverstein, R. L. (2000) Targeted disruption of the class B scavenger receptor CD36 protects against atherosclerotic lesion development in mice. *J. Clin. Invest.* **105,** 1049–1056
5. Mehta, J. L., Sanada, N., Hu, C. P., Chen, J., Dandapat, A., Sugawara, F., Satoh, H., Inoue, K., Kawase, Y., Jishage, K., Suzuki, H., Takeya, M.,

Schnackenberg, L., Beger, R., Hermonat, P. L., Thomas, M., and Sawamura, T. (2007) Deletion of LOX-1 reduces atherogenesis in LDLR knockout mice fed high cholesterol diet. *Circ. Res.* **100,** 1634–1642
6. Stary, H. C., Chandler, A. B., Glagov, S., Guyton, J. R., Insull, W., Jr., Rosenfeld, M. E., Schaffer, S. A., Schwartz, C. J., Wagner, W. D., and Wissler, R. W. (1994) A definition of initial, fatty streak, and intermediate lesions of atherosclerosis: a report from the Committee on Vascular Lesions of the Council on Arteriosclerosis, American Heart Association. *Circulation* **89,** 2462–2478
7. Cyrus, T., Witztum, J. L., Rader, D. J., Tangirala, R., Fazio, S., Linton, M. F., and Funk, C. D. (1999) Disruption of the 12/15-lipoxygenase gene diminishes atherosclerosis in apo E-deficient mice. *J. Clin. Invest.* **103,** 1597–1604
8. Gordon, S., and Martinez, F. O. (2010) Alternative activation of macrophages: mechanism and functions. *Immunity* **32,** 593–604
9. Yakubenko, V. P., Bhattacharjee, A., Pluskota, E., and Cathcart, M. K. (2011) $\alpha_M\beta_2$ integrin activation prevents alternative activation of human and murine macrophages and impedes foam cell formation. *Circ. Res.* **108,** 544–554
10. Folcik, V. A., Aamir, R., and Cathcart, M. K. (1997) Cytokine modulation of LDL oxidation by activated human monocytes. *Arterioscler. Thromb. Vasc. Biol.* **17,** 1954–1961
11. van Tits, L. J., Stienstra, R., van Lent, P. L., Netea, M. G., Joosten, L. A., and Stalenhoef, A. F. (2011) Oxidized LDL enhances pro-inflammatory responses of alternatively activated M2 macrophages: a crucial role for Kruppel-like factor 2. *Atherosclerosis* **214,** 345–349
12. Oh, J., Riek, A. E., Weng, S., Petty, M., Kim, D., Colonna, M., Cella, M., and Bernal-Mizrachi, C. (2012) Endoplasmic reticulum stress controls M2 macrophage differentiation and foam cell formation. *J. Biol. Chem.* **287,** 11629–11641
13. Khallou-Laschet, J., Varthaman, A., Fornasa, G., Compain, C., Gaston, A. T., Clement, M., Dussiot, M., Levillain, O., Graff-Dubois, S., Nicoletti, A., and Caligiuri, G. (2010) Macrophage plasticity in experimental atherosclerosis. *PLoS One* **5,** e8852
14. Yakubenko, V. P., Hsi, L. C., Cathcart, M. K., and Bhattacharjee, A. (2013) From macrophage interleukin-13 receptor to foam cell formation: mechanisms for $\alpha_M\beta_2$ integrin interference. *J. Biol. Chem.* **288,** 2778–2788
15. Xiong, Y. M., Chen, J., and Zhang, L. (2003) Modulation of CD11b/CD18 adhesive activity by its extracellular, membrane-proximal regions. *J. Immunol.* **171,** 1042–1050
16. Maglott, D., Ostell, J., Pruitt, K. D., and Tatusova, T. (2011) Entrez Gene: gene-centered information at NCBI. *Nucleic Acids Res.* **39,** D52-D57
17. Altschul, S. F., Madden, T. L., Schaffer, A. A., Zhang, J., Zhang, Z., Miller, W., and Lipman, D. J. (1997) Gapped BLAST and PSI-BLAST: a new generation of protein database search programs. *Nucleic Acids Res.* **25,** 3389–3402
18. Edgar, R. C. (2004) MUSCLE: a multiple sequence alignment method with reduced time and space complexity. *BMC. Bioinformatics* **5,** 113
19. Thompson, J. D., Higgins, D. G., and Gibson, T. J. (1994) CLUSTAL W: improving the sensitivity of progressive multiple sequence alignment through sequence weighting, position-specific gap penalties and weight matrix choice. *Nucleic Acids Res.* **22,** 4673–4680
20. Pazos, F., and Valencia, A. (2001) Similarity of phylogenetic trees as indicator of protein-protein interaction. *Protein Eng.* **14,** 609–614
21. Pazos, F., Ranea, J. A., Juan, D., and Sternberg, M. J. (2005) Assessing protein co-evolution in the context of the tree of life assists in the prediction of the interactome. *J. Mol. Biol.* **352,** 1002–1015
22. Sato, T., Yamanishi, Y., Kanehisa, M., and Toh, H. (2005) The inference of protein-protein interactions by co-evolutionary analysis is improved by excluding the information about the phylogenetic relationships. *Bioinformatics* **21,** 3482–3489
23. Zhang, L., and Plow, E. F. (1996) Overlapping, but not identical, sites are involved in the recognition of C3bi, neutrophil inhibitory factor, and adhesive ligands by the $\alpha_M\beta_2$ integrin. *J. Biol. Chem.* **271,** 18211–18216
24. Ehirchiou, D., Xiong, Y. M., Li, Y., Brew, S., and Zhang, L. (2005) Dual function for a unique site within the β_2I domain of integrin $\alpha_M\beta_2$. *J. Biol. Chem.* **280,** 8324–8331
25. Zhang, L., and Plow, E. F. (1997) Identification and reconstruction of the binding site within $\alpha_M\beta_2$ for a specific and high affinity ligand, NIF. *J. Biol. Chem.* **272,** 17558–17564
26. Cao, C., Lawrence, D. A., Li, Y., von Arnim, C. A., Herz, J., Su, E. J., Makarova, A., Hyman, B. T., Strickland, D. K., and Zhang, L. (2006) Endocytic receptor LRP together with tPA and PAI-1 coordinates Mac-1-dependent macrophage migration. *EMBO J.* **25,** 1860–1870
27. Li, A. C., Binder, C. J., Gutierrez, A., Brown, K. K., Plotkin, C. R., Pattison, J. W., Valledor, A. F., Davis, R. A., Willson, T. M., Witztum, J. L., Palinski, W., and Glass, C. K. (2004) Differential inhibition of macrophage foam-cell formation and atherosclerosis in mice by PPARα, β/δ, and γ. *J. Clin. Invest.* **114,** 1564–1576
28. Pazos, F., and Valencia, A. (2008) Protein co-evolution, co-adaptation and interactions. *EMBO J.* **27,** 2648–2655
29. Lovell, S. C., and Robertson, D. L. (2010) An integrated view of molecular coevolution in protein-protein interactions. *Mol. Biol. Evol.* **27,** 2567–2575
30. Kann, M. G., Shoemaker, B. A., Panchenko, A. R., and Przytycka, T. M. (2009) Correlated evolution of interacting proteins: looking behind the mirrortree. *J. Mol. Biol.* **385,** 91–98
31. Roy, B., Bhattacharjee, A., Xu, B., Ford, D., Maizel, A. L., and Cathcart, M. K. (2002) IL-13 signal transduction in human monocytes: phosphorylation of receptor components, association with Jaks, and phosphorylation/activation of Stats. *J. Leukoc. Biol.* **72,** 580–589
32. Maiguel, D., Faridi, M. H., Wei, C., Kuwano, Y., Balla, K. M., Hernandez, D., Barth, C. J., Lugo, G., Donnelly, M., Nayer, A., Moita, L. F., Schürer, S., Traver, D., Ruiz, P., Vazquez-Padron, R. I., Ley, K., Reiser, J., and Gupta, V. (2011) Small molecule-mediated activation of the integrin CD11b/CD18 reduces inflammatory disease. *Sci. Signal.* **4,** ra57
33. Wolf, D., Hohmann, J. D., Wiedemann, A., Bledzka, K., Blankenbach, H., Marchini, T., Gutte, K., Zeschky, K., Bassler, N., Hoppe, N., Rodriguez, A. O., Herr, N., Hilgendorf, I., Stachon, P., Willecke, F., Duerschmied, D., von zur Muhlen, C., Soloviev, D. A., Zhang, L., Bode, C., Plow, E. F., Libby, P., Peter, K., and Zirlik, A. (2011) Binding of CD40L to Mac-1's I-domain involves the EQLKKSKTL motif and mediates leukocyte recruitment and atherosclerosis — but does not affect immunity and thrombosis in mice. *Circ. Res.* **109,** 1269–1279
34. Cao, C., Gao, Y., Li, Y., Antalis, T. M., Castellino, F. J., and Zhang, L. (2010) The efficacy of activated protein C in murine endotoxemia is dependent on integrin CD11b. *J. Clin. Invest.* **120,** 1971–1980
35. Han, C., Jin, J., Xu, S., Liu, H., Li, N., and Cao, X. (2010) Integrin CD11b negatively regulates TLR-triggered inflammatory responses by activating Syk and promoting degradation of MyD88 and TRIF via Cbl-b. *Nat. Immunol.* **11,** 734–742
36. Adams, R. A., Bauer, J., Flick, M. J., Sikorski, S. L., Nuriel, T., Lassmann, H., Degen, J. L., and Akassoglou, K. (2007) The fibrin-derived $\gamma^{377-395}$ peptide inhibits microglia activation and suppresses relapsing paralysis in central nervous system autoimmune disease. *J. Exp. Med.* **204,** 571–582
37. Behrens, E. M., Sriram, U., Shivers, D. K., Gallucci, M., Ma, Z., Finkel, T. H., and Gallucci, S. (2007) Complement receptor 3 ligation of dendritic cells suppresses their stimulatory capacity. *J. Immunol.* **178,** 6268–6279
38. Ehirchiou, D., Xiong, Y., Xu, G., Chen, W., Shi, Y., and Zhang, L. (2007) CD11b facilitates the development of peripheral tolerance by suppressing Th17 differentiation. *J. Exp. Med.* **204,** 1519–1524
39. Flick, M. J., LaJeunesse, C. M., Talmage, K. E., Witte, D. P., Palumbo, J. S., Pinkerton, M. D., Thornton, S., and Degen, J. L. (2007) Fibrin(ogen) exacerbates inflammatory joint disease through a mechanism linked to the integrin $\alpha_M\beta_2$ binding motif. *J. Clin. Invest.* **117,** 3224–3235
40. Varga, G., Balkow, S., Wild, M. K., Stadtbaeumer, A., Krummen, M., Rothoeft, T., Higuchi, T., Beissert, S., Wethmar, K., Scharffetter-Kochanek, K., Vestweber, D., and Grabbe, S. (2007) Active MAC-1 (CD11b/CD18) on DCs inhibits full T-cell activation. *Blood* **109,** 661–669
41. Sohn, J. H., Bora, P. S., Suk, H. J., Molina, H., Kaplan, H. J., and Bora, N. S. (2003) Tolerance is dependent on complement C3 fragment iC3b binding to antigen-presenting cells. *Nat. Med.* **9,** 206–212
42. Hammerberg, C., Katiyar, S. K., Carroll, M. C., and Cooper, K. D. (1998) Activated complement component 3 (C3) is required for ultraviolet induction of immunosuppression and antigenic tolerance. *J. Exp. Med.* **187,** 1133–1138

43. Dandekar, T., Snel, B., Huynen, M., and Bork, P. (1998) Conservation of gene order: a fingerprint of proteins that physically interact. *Trends Biochem. Sci.* **23,** 324–328
44. Overbeek, R., Fonstein, M., D'Souza, M., Pusch, G. D., and Maltsev, N. (1999) Use of contiguity on the chromosome to predict functional coupling. *In Silico Biol.* **1,** 93–108
45. Enright, A. J., Iliopoulos, I., Kyrpides, N. C., and Ouzounis, C. A. (1999) Protein interaction maps for complete genomes based on gene fusion events. *Nature* **402,** 86–90
46. Goh, C. S., Bogan, A. A., Joachimiak, M., Walther, D., and Cohen, F. E. (2000) Co-evolution of proteins with their interaction partners. *J. Mol. Biol.* **299,** 283–293
47. Gertz, J., Elfond, G., Shustrova, A., Weisinger, M., Pellegrini, M., Cokus, S., and Rothschild, B. (2003) Inferring protein interactions from phylogenetic distance matrices. *Bioinformatics* **19,** 2039–2045
48. Pazos, F., Helmer-Citterich, M., Ausiello, G., and Valencia, A. (1997) Correlated mutations contain information about protein-protein interaction. *J. Mol. Biol.* **271,** 511–523
49. Xiong, J. P., Stehle, T., Zhang, R., Joachimiak, A., Frech, M., Goodman, S. L., and Arnaout, M. A. (2002) Crystal structure of the extracellular segment of integrin $\alpha_V\beta_3$ in complex with an Arg-Gly-Asp ligand. *Science* **296,** 151–155
50. LaPorte, S. L., Juo, Z. S., Vaclavikova, J., Colf, L. A., Qi, X., Heller, N. M., Keegan, A. D., and Garcia, K. C. (2008) Molecular and structural basis of cytokine receptor pleiotropy in the interleukin-4/13 system. *Cell* **132,** 259–272